

Morphologies in anisotropic cluster growth: A Monte Carlo study on Ag(110)

R. Ferrando, F. Hontinfinde,* and A. C. Levi

*Istituto Nazionale per la Fisica della Materia and Centro di Fisica delle Superfici e delle Basse Temperature del CNR,
Dipartimento di Fisica dell'Università di Genova, via Dodecaneso 33, 16146 Genova, Italy*

(Received 5 June 1997)

A model with deposition, diffusion, and reversible aggregation on a two-dimensional rectangular lattice with both anisotropic diffusion barriers and anisotropic nearest-neighbor bonds is studied by kinetic Monte Carlo simulations. The model is applied to the case of Ag growth on Ag(110). The barriers for the elementary processes are calculated by many-body tight-binding potentials. At fixed T decreasing the flux (or at fixed flux and increasing T), the model displays morphology changes from small isotropic aggregates to one-dimensional strips and then to two-dimensional islands. [S0163-1829(97)52732-9]

The experimental investigation of the morphologies of two-dimensional (2D) nanostructures,^{1,2} obtained by diffusion-controlled aggregation on metal surfaces,^{3,4} has recently stimulated much theoretical work. Models of 2D cluster growth with deposition, diffusion, and irreversible aggregation (DDA model⁵) have been thoroughly studied by kinetic Monte Carlo (KMC) simulations in both square^{6,7} and rectangular^{1,6} symmetries. The mobility of clusters as rigid bodies has been incorporated in the DDA model by different groups.^{8,9}

For reversible aggregation, the island morphologies have been studied by introducing edge diffusion¹⁰ without detachment. In this way, both fractal-like (at high fluxes) and compact island (at slow deposition rates) have been obtained. A model with fully reversible aggregation has been proposed by Ratsch *et al.*¹¹ for cluster growth in an isotropic model on a square lattice. In that model the scaling properties of island and adatom densities have been investigated depending on coverage θ , deposition rate, and temperature T .

In this paper, we propose a model with deposition, diffusion, and fully reversible aggregation on a rectangular substrate: the model, anisotropic both in the diffusion barriers of isolated adatoms and in the bonds between neighboring adatoms, is applied to the case of the low θ homoepitaxial growth of Ag(110). It is shown that, at fixed T , the morphology of the clusters grown on the substrate changes dramatically with the flux: at fast deposition rates, small isotropic clusters are formed; in the intermediate regime, well-separated one-dimensional strips along the in-channel $[1\bar{1}0]$ direction are formed; finally, at slow deposition rates, (2D) anisotropic islands grow. The same morphology changes are found at fixed deposition rate by increasing T . The morphology change from one-dimensional to 2D islands has been observed by scanning tunnel microscopy in the low-coverage deposition of Cu on Pd(110) by increasing T .³ We show that such changes are due to the anisotropy of bonds and to the possibility of in-channel bond breaking, the anisotropy of diffusion playing a minor role, contrary to what is assumed in Ref. 12. The study of the key factors determining the clusters shapes is essential in the fields of crystal growth and atomic manipulations.

The energy barriers are calculated^{13,14} by quenched molecular-dynamics simulations. In Ref. 14 a detailed dis-

cussion of the diffusive processes on Ag(110) at the atomic level can be found. Ag is modeled by many-body potentials as derived by Rosato, Guillopé, and Legrand (RGL).¹⁵ Concerning diffusion barriers on Ag surfaces, RGL potentials are in good agreement with experimental results as well as with other theoretical methods. For instance, on Ag(100) the experimental barrier is of 0.40 ± 0.05 eV,¹⁶ *ab initio* calculations give 0.45 eV (Ref. 17) while RGL potentials give 0.42 eV. On Ag(110), corrected effective-medium calculations¹⁸ give 0.26 eV for in-channel diffusion and 0.34 eV for cross-channel exchange, against 0.28 and 0.38 eV from RGL.

In our model atoms, deposited randomly at a rate F onto a rectangular substrate, can diffuse, aggregate, and dissociate. Data are taken when the final θ is reached. The transition rates are assumed to have the Arrhenius form $\nu \exp(-E_{p,n}/k_B T)$, where the subscripts p and n correspond to the parallel ($[1\bar{1}0]$) and normal ($[001]$) directions with respect to the atomic channels of the (110) surface. For simplicity, the prefactors ν are chosen to be the same for all diffusion processes. The barriers $E_{p,n}$ for the different diffusion processes depend both on the direction of the move and on the numbers of neighbors of the moving adatom:

$$E_p = E_p^0 + n_p E_p^b + n_n E_n^b, \quad (1)$$

$$E_n = E_n^0 + n_p E_p^b + n_n E_n^b; \quad (2)$$

$E_{p,n}^0$ are the barriers for diffusion on the bare surface; $E_{p,n}^b$ and $n_{p,n}$ are the strengths and numbers of in-channel and cross-channel bonds. This form of the energy barriers is an approximation, as they are assumed to depend only on the neighbors in the initial configuration. However, for the (110) surface this approximation is very good, as it reproduces to a high degree of accuracy the results in Ref. 14, where the energy barriers have been calculated taking into account the full environment of the diffusing adatom. This approximation is not appropriate, however, for the fcc(100) surface, where, for instance, enhanced diffusion along straight steps must be taken into account.^{19,20} However, for Ag(110), we did not find such enhanced diffusion.¹⁴ Moreover, the barriers for motion towards island edges are not significantly lower than the ones for adatom diffusion on the flat

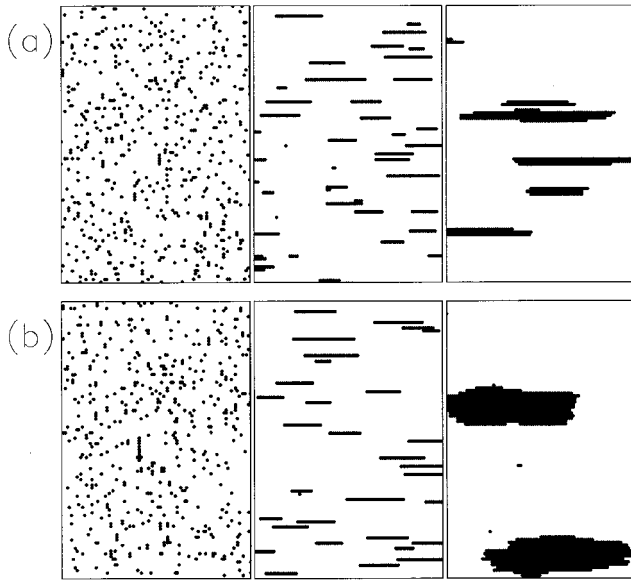


FIG. 1. Typical island morphologies for (100 rows \times 100 columns) sections of (300 \times 300) simulations. The horizontal direction is the in-channel [110] direction. (a) Upper panels: morphologies at fixed $T=200$ K and final coverage ($\theta=0.05$) but with different Γ . The left, middle, and right panels correspond to $\Gamma=10^2$, 2×10^7 and 5×10^9 , respectively. (b) Lower panels: morphologies at fixed deposition rate F (of about 0.1 layers per minute, see the text) and $\theta=0.05$ but with different T . The left, middle, and right panels correspond to $T=110$, 200, and 275 K, respectively. At 275 K few large compact islands grow. Two of them are shown in the snapshot.

surface.¹⁴ Depending on the direction of diffusion and the number of bonds, 12 processes are possible plus deposition. As we are interested in low θ ($\theta \leq 0.05$), we neglect the possibility of depositing adatoms onto pre-existing islands.⁸ The KMC simulations have been performed by the algorithm of Bortz *et al.*^{21,22} and many checks have been made in order to ensure the convergence of the results with system size.²³

From RGL calculations,¹⁴ the following choice is appropriate:

$$(A) \quad E_p^0 = 0.28, \quad E_n^0 = 0.38, \quad E_p^b = 0.18, \quad E_n^b = 0.02 \text{ eV.}$$

Cross-channel diffusion occurs by exchange,^{13,18} since the barrier for the cross-channel jump is very high [~ 0.8 eV (Refs. 13 and 14)]. Dimers and larger clusters are assumed not to move as rigid bodies. We have calculated the diffusion barrier for an in-channel dimer finding that it is much larger than the one for adatom diffusion. In the following, most results are presented as a function of $\Gamma = D/F$, where D is the hopping rate in the in-channel direction.

In Fig. 1, the morphologies of the clusters depending on Γ and T are presented. In the upper panels, T is fixed at 200 K and Γ takes the values 10^2 , 2×10^7 and 5×10^9 from left to right. At low Γ (high flux), the aggregates are small and no preferential direction in their orientation is observed. In the intermediate case, well-separated one-dimensional strips in the in-channel direction are formed. At high Γ , the islands are still anisotropic but two dimensional. In the lower panels, the flux F is fixed and T is changed: 110, 200, and 275 K from left to right. If we assume a prefactor $\nu = 10^{12} \text{ s}^{-1}$, F

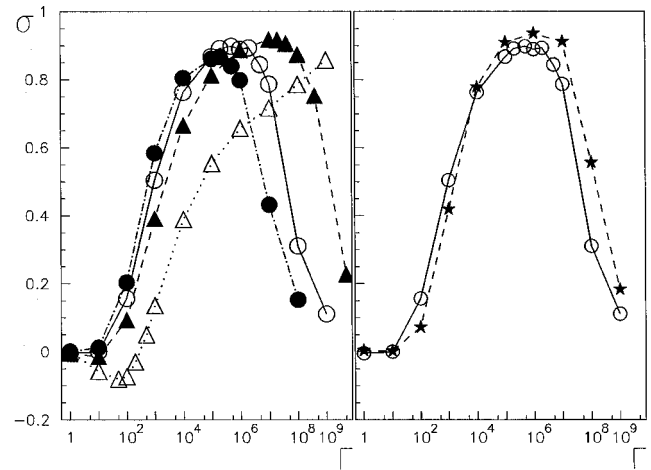


FIG. 2. Left panel: anisotropy parameter σ vs Γ , at fixed $\theta=0.05$ for different temperatures: 110 K (white triangles), 200 K (black triangles), 250 K (open circles), and 300 K (black circles). Right panel: σ vs Γ , at fixed temperature ($T=250$ K) for different final coverages: $\theta=0.025$ (black stars) and $\theta=0.05$ (open circles).

corresponds to 0.1 monolayers per minute. At 200 K almost all islands are long in-channel strips; on the contrary, at 275 K we obtain few compact aggregates. The results at 200 and 275 K resemble closely those obtained in Cu/Pd(110) at 300 and 350 K, respectively.³ In our case, the crossover from monatomic strips to compact aggregates happens in a temperature interval of about 30 K. At this flux, the average width of the islands in the cross-channel direction is of 1.1, 2.3, and 4.6 lattice spacings at 200, 230, and 250 K, respectively. At 110 K, the islands have a slight preference for orientation in the cross-channel direction.

In order to characterize the degree of anisotropy and compactness of the islands, we introduce the parameter

$$\sigma = \frac{\bar{n}_p - \bar{n}_n}{\bar{n}_p + \bar{n}_n}; \quad (3)$$

$\bar{n}_{p,n}$ are the average number of parallel and normal nearest-neighbor bonds at a given Γ , T , and θ . σ approaches 1 only if the islands are one-dimensional in-channel strips (no cross-channel bonds); in the case of 2D islands, σ is small. The results for σ versus Γ are reported in Fig. 2, at $\theta=0.05$ and $T=110$, 200, 250, and 300 K (left panel), and at $T=250$ K and $\theta=0.025$ and 0.05 (right panel). The three regimes (small isotropic clusters, monatomic strips, and 2D islands) can be easily identified. Moreover, at the lowest T , there is a low- Γ regime where the anisotropy is slightly reversed ($\sigma < 0$).

The physical picture leading to the three regimes may be sketched as follows. For instance, let us fix T and vary Γ . At low Γ , cross-channel diffusion does not occur. Islands are small, many atoms are isolated. Under those conditions, it is more likely that an isolated adatom will make its first encounter with a cross-channel neighbor (it can find cross-channel neighbors in both adjacent channels, in-channel neighbors only in its own channel). At low T , cross-channel bonds are rather stable, although less than in-channel bonds. Depending on the degree of stability of cross-channel bonds,

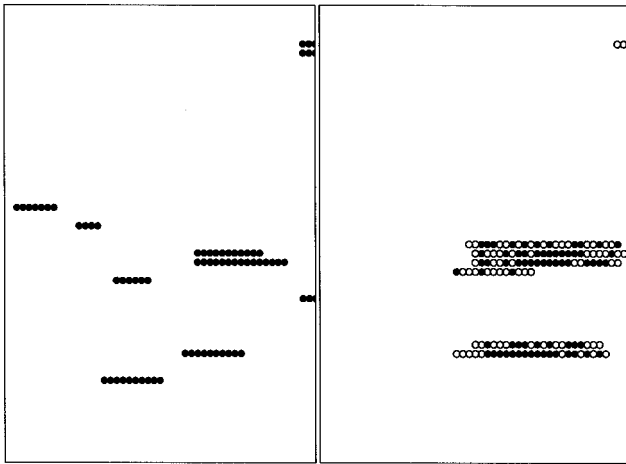


FIG. 3. (50×50) sections of the same (200×200) simulation at $T=250$ K and $\Gamma=10^8$. The left snapshot is taken after the first half of the simulation, i.e., after the deposition of 1000 atoms ($\theta=0.025$, 72 atoms are in the section); the right snapshot is taken at the end of the simulation, i.e., after the deposition of 2000 atoms ($\theta=0.05$, 136 atoms are in the section). The atom deposited in the first half of the simulation are represented by black circles, the others by open circles.

there may be a slight reversal in the anisotropy of clusters (as it happens at 110 K) or no anisotropy at all. At intermediate Γ , both in-channel and cross-channel diffusion are possible; cross-channel bonds are no more stable, while in-channel bonds are still stable. These conditions lead to the formation of monatomic strips. At high Γ , even in-channel bonds can be broken. Island dissolution becomes important; on the average, small islands and monatomic strips disappear in favor of more compact (and energetically more stable) clusters. This can be seen in Fig. 3, where two snapshots of the same simulation (at $T=250$ K and $\Gamma=10^8$) at different times are shown. The snapshot on the left is taken after the deposition of half of the atoms (corresponding to $\theta=0.025$) and the one on the right is taken at the end of the simulation ($\theta=0.05$). The atoms deposited in the first half of the simulation are represented by black circles, those deposited in the second half by open circles. Clearly, a large part of the monatomic strips of the left panel has disappeared at the end of the simulation; one of the 2D islands has grown considerably with rather complicated rearrangements.

In order to confirm the above picture, we consider different choices of the energy parameters. In choice (B) the bonds are anisotropic as in (A), but diffusion is isotropic:

$$(B) \quad E_p^0=0.28, \quad E_n^0=0.28, \quad E_p^b=0.18, \quad E_n^b=0.02 \text{ eV};$$

in choice (C) diffusion is anisotropic as in (A) but the bonds are isotropic and strong:

$$(C) \quad E_p^0=0.28, \quad E_n^0=0.38, \quad E_p^b=0.18, \quad E_n^b=0.18 \text{ eV};$$

in choice (D), diffusion barriers and cross-channel bonds are as in (A), but the possibility of breaking in-channel bonds is suppressed:

$$(D) \quad E_p^0=0.28, \quad E_n^0=0.38, \quad E_p^b=\infty, \quad E_n^b=0.02 \text{ eV}.$$

The results of the above choices are presented in Fig. 4 at

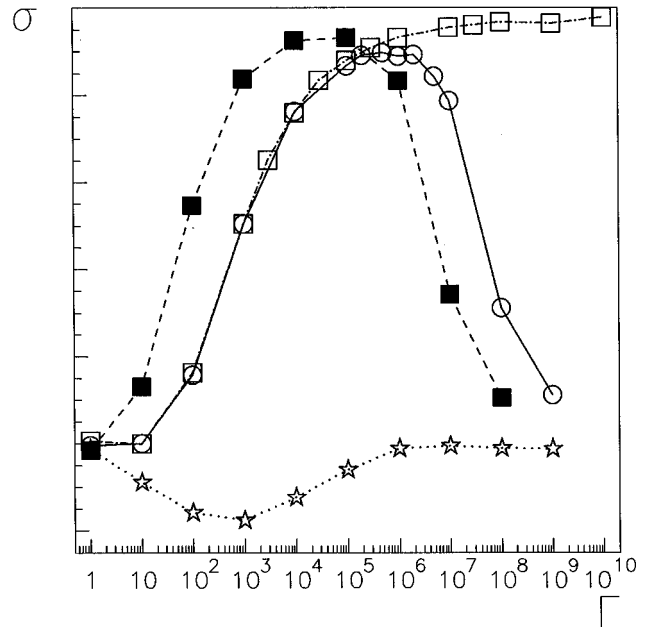


FIG. 4. Anisotropy parameter σ vs Γ at fixed $T=250$ K and $\theta=0.05$ for different energy barrier choices (see text): (A) (open circles), (B) (black squares), (C) (white stars), and (D) (open squares).

$T=250$ K and $\theta=0.05$, and compared to those for choice (A) (open circles). The introduction of isotropic diffusion [choice (B), black squares] has the only effect of shifting the maximum to lower Γ ; one-dimensional in-channel strips are still obtained. At low T , it can be seen that the low- Γ inversion of the anisotropy is suppressed in choice (B). The introduction of strong isotropic bonds [choice (C), white stars] has more dramatic effects on the morphologies. The anisotropy is weak but is reversed; in the low- Γ regime where islands are small, cross-channel diffusion is negligible and all bonds are stable. The regime of the one-dimensional in-channel strips is not obtained. Thus the isotropy or anisotropy of bonds is crucial for the island morphologies.²⁴ Finally, it can be seen that, by suppressing the in-channel-bond breaking [choice (D), open squares], the transition to 2D islands does not take place, at least up to $\Gamma=10^{10}$. Therefore, the mechanisms governing the morphology changes are quite different from the ones proposed to explain the morphology transitions on Cu/Pd(110) in Ref. 12. There, the morphology changes were attributed to the diffusion anisotropy with irreversible attachment. On the contrary, we have shown here that the growth of monatomic strips is due to the anisotropy of bonds and not to the absence of cross-channel diffusion; the transition to 2D clusters is due to the onset of in-channel bond breaking and not to the onset of cross-channel diffusion (the latter being already effective at lower Γ). Diffusion anisotropy and irreversible attachment in both directions cannot produce the observed effects.

In conclusion, our simulations have shown that the morphologies of clusters grown at low-coverage deposition on Ag(110) varies from small isotropic clusters to well-defined strips of monatomic width in the in-channel direction and to 2D anisotropic islands, depending on flux and on T . At very low T , there is a regime where the anisotropy of clusters is slightly reversed (the cross-channel orientation is preferred).

The growth of monatomic strips is possible because of the anisotropy between in-channel and cross-channel bonds, whereas the transition to 2D islands happens on the time scale at which in-channel-bond dissociation becomes important.

Useful discussions with Dr. D. Cvetko, L. Floreano, P. Ruggerone and E. Scalas are acknowledged. One of the authors (F.H.) acknowledges financial support from the ICTP Program for Training and Research in Italian laboratories.

*On leave from: LPT/LMPHE, Faculté des Sciences, BP1014 Rabat, Morocco and IMSP, Université Nationale du Benin, BP 613 P. Novo, Benin.

¹Y. W. Mo, J. Kleiner, M. B. Webb, and M. Lagally, Phys. Rev. Lett. **66**, 1998 (1991).

²J. A. Strosio, D. T. Pierce, and R. A. Dragoset, Phys. Rev. Lett. **70**, 3615 (1993).

³H. Röder, E. Hahn, H. Brune, J. P. Bucher, and K. Kern, Nature (London) **366**, 141 (1993); K. Kern, E. Hahn, E. Kampshoff, A. Fricke, and J. P. Bucher, Surf. Sci. **319**, 277 (1994).

⁴T. Michely, M. Hohage, M. Bott, and G. Comsa, Phys. Rev. Lett. **70**, 3943 (1993).

⁵A.-L. Barabási and H. E. Stanley, *Fractal Concepts in Surface Growth* (Cambridge University Press, Cambridge, 1995).

⁶M. C. Bartelt and J. W. Evans, Phys. Rev. B **46**, 12 675 (1992); Europhys. Lett. **21**, 99 (1993).

⁷J. G. Amar, F. Family, and P. M. Lam, Phys. Rev. B **50**, 8781 (1994).

⁸P. Jensen, A.-L. Barabási, H. Larralde, S. Havlin, and H. E. Stanley, Phys. Rev. E **50**, 618 (1994); Phys. Rev. B **50**, 15 316 (1994).

⁹L. Kuipers and R. E. Palmer, Phys. Rev. B **53**, 7646 (1996).

¹⁰G. S. Bales and D. C. Chrzan, Phys. Rev. B **50**, 6057 (1994); S. Liu, Z. Zhang, G. Comsa, and H. Metiu, Phys. Rev. Lett. **71**, 2967 (1993); M. C. Bartelt and J. W. Evans, Surf. Sci. **314**, L829 (1994).

¹¹C. Ratsch, A. Zangwill, P. Šmilauer, and D. D. Vvedensky, Phys. Rev. Lett. **72**, 3194 (1994).

¹²J. P. Bucher, E. Hahn, P. Fernandez, C. Massobrio, and K. Kern, Europhys. Lett. **27**, 473 (1994).

¹³R. Ferrando, Phys. Rev. Lett. **76**, 4195 (1996).

¹⁴R. Ferrando, F. Hontinfinde, and A. C. Levi, Surf. Sci. **366**, 306 (1996).

¹⁵V. Rosato, M. Guillopé, and B. Legrand, Philos. Mag. A **59**, 321 (1989).

¹⁶M. H. Langelaar, M. Breeman, and D. O. Boerma, Surf. Sci. **352-354**, 597 (1996).

¹⁷B. D. Yu and M. Scheffler, Phys. Rev. Lett. **77**, 1095 (1996).

¹⁸L. S. Perkins and A. E. DePristo, Surf. Sci. **317**, L1152 (1994).

¹⁹A. F. Voter, Phys. Rev. B **34**, 6819 (1986).

²⁰G. T. Barkema, O. Biham, M. Breeman, D. O. Boerma, and G. Vidali, Surf. Sci. **306**, L569 (1994).

²¹A. B. Bortz, M. H. Kalos, and J. L. Lebowitz, J. Comp. Phys. **17**, 10 (1975); P. A. Maksym, Semicond. Sci. Technol. **3**, 594 (1988).

²²A. C. Levi and M. Kotrla, J. Phys. Condens. Matter **9**, 299 (1997).

²³K. R. Roos and M. C. Tringides, Surf. Sci. **355**, L259 (1996).

²⁴Y. T. Lu and H. Metiu, Surf. Sci. **245**, 150 (1991); Y. T. Lu, P. Petroff, and H. Metiu, Appl. Phys. Lett. **57**, 2683 (1990).